A Multi-Attribute Adaptive Fault Diagnosis Framework for Star Networks

Wenfei Liu, Jiafei Liu, Eddie Cheng, Sun-Yuan Hsieh, *Fellow, IEEE*, Jingli Wu, and Gaoshi Li

***Abstract*—With the proliferation of interconnection networks in mission-critical systems ranging from cloud computing infrastructures to large-scale data centers, the escalating structural complexity has intensified network vulnerability to malicious attacks and cyber warfare incidents. This article establishes a theoretical framework for evaluating network self-diagnostic capability through a novel h-extra r-component diagnosability metric, denoted as $\widehat{ec}_r^h(G)$, which quantifies a network's resilience under compound fault patterns. The proposed metric requires that after removing specific nodes, the remaining subgraph is required to preserve at least r connected components where every component maintains a node count exceeding h. Through rigorous combinatorial analysis, we derive closed-form expressions for star networks S_n, $\widehat{ec}_2^1(S_n) = 4n - 9$ and $\widehat{ec}_3^1(S_n) = 6n - 15$ when $n \geq 6$, establishing the tight diagnosability bounds for this fundamental network topology. To enable practical implementation, we design a Trial System-based Fault Diagnosis Algorithm (TSFD) that features adaptive syndrome verification and parallel fault localization mechanisms. Extensive simulations demonstrate the accuracy of 98.99% fault detection with linear-time complexity $O(Nd)$ in n-dimensional star networks. This work advances network reliability theory by introducing a multi-feature diagnosability measure for system-level diagnosis and developing an efficient diagnosis algorithm validated through large-scale network emulation.**

***Index Terms*—Star graph, h-extra r-component diagnosability, PMC model, fault diagnosis.**

Received 31 May 2025; revised 10 September 2025; accepted 19 October 2025. Date of publication 24 October 2025; date of current version 11 December 2025. This work was supported in part by the National Natural Science Foundation of China under Grant 62302107 and Grant 62366007; in part by Guangxi Natural Science Foundation under Grant 2025GXNSFBA069563 and Grant 2025GXNSFAA069507; in part by Research Fund of Guangxi Key Lab of Multi source Information Mining Security under Grant 24-A-03-01; in part by the Basic Ability Enhancement Program for Young and Middle-Aged Teachers of Guangxi, China under Grant 2023KY0063; in part by the Young Elite Scientists Sponsorship Program by GXAST under Grant 2025YESSGX010; and in part by the Innovation Project of Guangxi Graduate Education under Grant XYCS2025121. Recommended for acceptance by D. Bertozzi. *(Corresponding author: Jiafei Liu.)*

Wenfei Liu, Jiafei Liu, Jingli Wu, and Gaoshi Li are with the Key Lab of Education Blockchain and Intelligent Technology, Ministry of Education, Guangxi Normal University, Guilin 541004, China, also with Guangxi Key Lab of Muli-Source Information Mining and Security, Guangxi Normal University, Guilin 541004, China, and also with the Center for Applied Mathematics of Guangxi, Guangxi Normal University, Guilin 541004, China (e-mail: liuwenfei@stu.gxnu.edu.cn; liujiafei@gxnu.edu.cn; wjhappy@gxnu.edu.cn; ligaoshi@mailbox.gxnu.edu.cn).

Eddie Cheng is with the Department of Mathematics and Statistics, Oakland University, Rochester, MI 48309 USA (e-mail: echeng@oakland.edu).

Sun-Yuan Hsieh is with the Department of Computer Science and Information Engineering, National Cheng Kung University, Tainan 701, Taiwan (e-mail: hsiehsy@mail.ncku.edu.tw).

Digital Object Identifier 10.1109/TC.2025.3624839

I. Introduction

THE proliferation of cyber-physical systems (CPS) and Internet-of-Things (IoT) ecosystems has created mission-critical dependencies on high-availability interconnection networks. Modern organizational networks utilize the synergistic integration of SDN controllers and NFV-based virtualized network services to achieve centralized orchestration of geographically dispersed infrastructure domains, yet these technologies introduce unprecedented architectural complexity. The expanding attack surface manifests through two critical dimensions: (1) Vertical heterogeneity - with 54 billion IoT devices projected by 2025 (IDC 2023) spanning edge-to-cloud layers, and (2) Horizontal dynamism - requiring real-time reconfiguration of 5G network slices and microservice-based applications. This complexity amplifies vulnerability to multi-vector cyber threats, as evidenced by a great increase in state-sponsored DDoS attacks(Gartner 2023) capable of generating 3.5 Tbps malicious traffic. System-level fault diagnosis has emerged as a critical requirement for next-generation networks, particularly in interconnection networks and data center networks.

Network architecture generally refers to the underlying topological structure of a network. This means that during the design and implementation of network architecture, it is essential to focus on improving the fault tolerance and self-diagnostic efficiency. This ensures that when faults arise during network operation, the problems can be quickly and accurately identified, allowing for prompt and effective solutions. Based on exploration of network architecture, in 1989, Akers and Krishnamurthy [1] introduced the star graph S_n using a graph theory model as a bridge. This structure has a series of advantages, including high bandwidth, low latency, and scalability, which makes it a popular subject of research. As early in 1967, Preparata et al. [2] proposed a diagnostic model applied to chip testing, known as the PMC. This is a test-based diagnostic model where neighboring processors test each other, generating a set of symptoms for diagnosis. The classic diagnosability is an indicator initially used by researchers to measure the self-diagnostic performance of a network. It represents the maximum number of faulty nodes the system can identify.

However, there is a limitation in classical diagnosability: the probability of all adjacent nodes of a processor failing simultaneously is extremely low, which does not correspond to real-world scenarios. Therefore, Cheng et al. [3] introduced the concept of conditional diagnosability. It adds conditions to the structure of the remaining subgraph after some nodes are

removed from a connected graph, preventing the occurrence of isolated nodes. Building on conditional diagnosability, Zhang and Yang [4] introduced the g-extra conditional diagnosability framework, mandating that every connected subgraph remaining after fault removal contains no fewer than $h+1$ nodes per component. In this case, the maximum number of identifiable faulty nodes in the system is referred to as h-extra diagnosability. Subsequently, more diagnosability strategy has been proposed. Li et al. [5] investigated the 3-extra conditional diagnosability of balanced hypercubes based on the MM$*$ model. Zheng et al. [6] studied the non-inclusive g-extra diagnosability of a class of networks under the PMC model. Cheng and Lipták [7] studied the connectivity of the Cayley graphs generated by the permutation tree after removing a linear number of vertices, and proved that it still retains a large universal component. Cheng and Lipták [8] studied the fault tolerance of Cayley graphs generated by permutation and proved that they could still maintain connections or only have a few small components after deleting a large number of vertices. Lin et al. [9] proved the t/k-diagnosticability theoretical boundary of the regular network G that satisfies specific conditions and established the effectiveness of the diagnostic algorithm. Lin et al. [10] proposed the H-faulty-block connectivity metric model based on the dispersion of remaining nodes to resist block attacks. Tian et al. [11] examined the extra diagnosability of hypercubes under the bounded PMC model. In 2022, Zhang et al. [12] introduced the concept of component diagnosability. They defined that there be at least r components in the remaining subgraph. In this case, the maximum number of identifiable faulty nodes in the system is referred to as r-component diagnosability. Zhuang et al. [13], [14] studied the component diagnosability of general networks and data center networks. Huang et al. [15] established diagnostic thresholds for fault detection in hierarchical cube networks, formalizing criteria to ensure operational resilience across layered components under system failures. Liu et al. [16] studied the component diagnosability of a class of topologies based on hypercube networks using component connectivity as a bridge. Tian and Zhu [17] studied the component diagnosability of hypercube.

Currently, there are some recent research findings in the network's ability to self-diagnosis. Peng et al. [18] introduced g-good diagnosability. Fan et al. [19] constructed a fault-tolerant routing algorithm based on node disjoint multipath to enhance the fault-tolerant capability of the BCube network. Lin et al. [20] has expanded the theoretical boundaries of multipath fault tolerance in server-centralized networks under complex fault modes. Zhang et al. [21] introduced cyclic diagnosability of regular networks. Huang et al. [22] established an adaptive system-level fault diagnosis strategy for bijective connection networks. Lin et al. [23] employed new neural network techniques for intermittent fault diagnosis. Song et al. [24] presented an efficient fault diagnosis algorithm to address the intermittent fault distribution of interconnection networks. Lv et al. [25] analyzed the fault tolerance performance of complete cubic networks based on extra conditional faults. Yang et al. [26] explored the (t,k)-diagnosability of Cayley graph generated by 2-trees under different diagnostic models.

Existing problems: Existing network fault diagnosis methods in current research predominantly focus on single conditions, making it difficult to reflect the complexity of fault distribution in real-world network environments. In large-scale parallel distributed systems, network partition events caused by human interference or hacker attacks are not uncommon. Previous diagnosability studies, including classical diagnosability, component diagnosability, and extra diagnosability, primarily concentrate on the quantity or scale of partitions while lacking a comprehensive evaluation of the system's self-diagnostic capability. To address this gap, this paper proposes the h-extra r-component diagnosability ($\widehat{ec}_r^h(G)$) metric, which integrates the strengths of existing methods by simultaneously considering both the scale and quantity of components in the network, thereby providing a more holistic assessment of the system's fault tolerance. Furthermore, the Star Graph, due to its unique topological properties, demonstrates significant application potential in structured topology scenarios such as high-performance computing clusters, distributed storage systems, and data center networks, further enhancing the engineering significance and practicality of this study. The following sections detail the contributions of this study.

1) **Research on h-Extra r-Component Diagnosability**: We present a novel fault identification scheme on h-extra r-component diagnosability and have completed the theoretical proofs for $\widehat{ec}_2^1(S_n)$ and $\widehat{ec}_3^1(S_n)$ using the PMC model.
2) **Design of Trial System-based Fault Diagnosis Algorithm (TSFD):** We design a fault diagnosis algorithm based on a trial system to improve diagnosis efficiency. By simulating different fault scenarios, the algorithm quickly identifies faults and locates problems, reducing diagnosis time and improving system reliability.
3) **Experimental Verification of Algorithm Performance:** Through simulation experiments, we evaluate the performance of the TSFD algorithm in S_n, demonstrating its superiority in fault detection.

The organization of this paper is developed as follows. In Section II, we provide a detailed explanation of the preliminaries for this paper, covering the basic concepts of graph theory, the properties of star graphs, and an overview of the PMC diagnostic model. In Section III, we present a comprehensive proof of the h-extra r-component diagnosability, specifically including the derivations for $\widehat{ec}_2^1(S_n)$ and $\widehat{ec}_3^1(S_n)$. Section IV focuses on introducing our fault diagnosis algorithm designed based on the trial system, and we verify its effectiveness and performance through a series of simulation experiments. Section V conducts some discussions and practical application experiments on the algorithm proposed in this paper. Finally, in Section VI, we summarize the entire paper.

II. Preliminaries

In this section, we will present some terminology and concepts necessary for this paper.

A. Terminologies and Notions

Interconnection network topology, as an abstract representation of the network structure, is often described by a graph $G = (V, E)$, where nodes in the graph correspond to the actual units, and edges represent the communication links between units.

Given a graph G, its node set is usually denoted by V and its edge set is usually denoted by E. In this paper, we are only interested in graphs where edges have no directions and every edge has two distinct end nodes. A traversal sequence $(v_1, v_2, \ldots, v_k)$ forms a path whose length corresponds to its edge count, while a closed traversal with identical start and end nodes constitutes a cycle. Let S_1 and S_2 be two subsets of nodes of G, and define the edge set $E(S_1, S_2)$ as the set of all edges connecting S_1 and S_2, i.e., $E(S_1, S_2) = \{(u, v) \in E(G) \mid \exists u \in S_1, \exists v \in S_2\}$. An l-path has length l, denoted P_l, while an l-cycle is denoted by C_l. The girth of a graph is the length of its shortest cycle, denoted $g(G)$. The open neighbor set of a node v, $N_G(v)$, includes all nodes adjacent to v, defined as $N_G(v) = \{u \in V | (u, v) \in E\}$. The closed neighbor set is $N_G[v] = N_G(v) \cup \{v\}$. The degree of a node v, $d_G(v)$, is the number of neighbors it has. The minimum degree of a graph is given by $\delta(G) = \min\{d_G(u) | u \in V(G)\}$. A graph is n-regular if every node has degree n. A node cut F is a nonempty subset that, when removed, makes the graph disconnected. A component is the maximal connected subgraph after removing F. An induced subgraph from a set S, denoted $G[S]$, includes the nodes in S and edges between them. The open neighbor set of a set S is $N_G(S) = \{v \in V \setminus S | \exists u \in S, (u, v) \in E\}$, and the closed neighbor set is $N_G[S] = N_G(S) \cup S$. The difference set $F_1 - F_2$ includes nodes in F_1 but not in F_2, and the symmetric difference $F_1 \Delta F_2$ combines the nodes in two sets excluding their intersection. Lastly, the Hamming distance $H(x, y)$ counts how many bits differ between two binary sequences x and y.

B. The Star Graph

The n-dimensional star graph S_n is a favorable candidate for interconnection networks, which has the advantages of low degree, small diameter, symmetry, and hereditary. An overview of the structural attributes and fundamental properties characterizing the n-dimensional star graph S_n is provided as follows:

Definition 1 [1]: As a Cayley graph, the n-dimensional star graph S_n (depicted in Fig. 1) exhibits:

1) Node set: $V = \{x \mid x \text{ is a permutation of } [n]\}$;
2) Edge set: $E = \bigcup_{i=2}^{n} \{(x, x_{(1 \leftrightarrow i)}) \mid x \in V\}$, where $x_{(1 \leftrightarrow i)}$ indicates the permutation obtained by swapping the 1st and i -th elements of x.

Lemma 1 [27]: The star graph S_n exhibits the subsequent characteristics:

1) In S_n, the number of nodes equals $n!$, and the graph is $(n-1)$ -regular, ensuring all vertices share the same degree.
2) S_n can be partitioned into n disjoint subgraphs, each characterized by fixing a distinct element i at the terminal position, denoted by $S_n^1, S_n^2, \ldots, S_n^n$ respectively, such that $S_n^i \cong S_{n-1} (i \in \langle n \rangle)$.
3) For distinct subgraphs S_n^i and S_n^j $(i \neq j \in \langle n \rangle)$, the interconnecting edges form a set $E(i, j)$, whose cardinality satisfies $|E(i, j)| = (n-2)!$.
4) For all $n \geq 3$, the shortest cycle in S_n has length 6, establishing its girth as $\text{girth}(S_n) = 6$.
5) Every pair of distinct nodes shares at most one common neighbor.

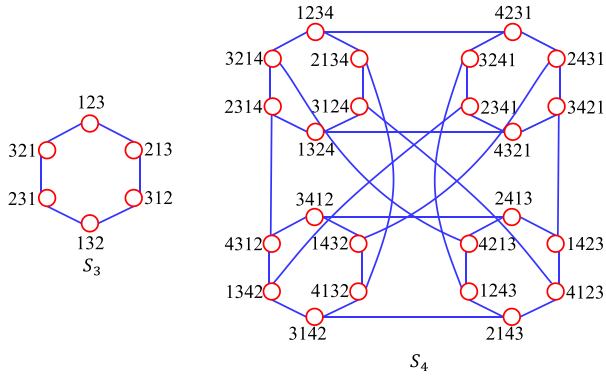

Fig. 1. Star graph.

C. System-Level Diagnostics

Next, we introduce some concepts and lemmas of system-level diagnostics.

Definition 2 [2]: The definition of the PMC model can be summarized. Let u and v be processors in a multiprocessor system, where u tests v. The test result as follows:

$$\sigma(u, v) = \begin{cases} 0, & \text{under the condition that nodes } u, v \notin F \\ 1, & \text{under the condition that nodes } v \in F \\ 0/1, & \text{under the condition that nodes } u \in F \end{cases}$$

Lemma 2 [2]: A pair of distinct subsets $(F_1, F_2) \subseteq V(G)$ is distinguishable if there exists:

- a node $u \in V(G) \setminus (F_1 \cup F_2)$;
- a node $v \in F_1 \triangle F_2$,

such that the edge (u, v) is present in $E(G)$. When no such pair (u, v) exists, the subsets F_1 and F_2 are indistinguishable.

Next, we introduce some key definitions and lemmas.

Definition 3 [28]: In a system G, a node subset $F \subseteq V(G)$ is termed an h-extra r-component fault set (denoted as $\mathcal{F}_r^h(G)$) if the removal of F from G produces a residual graph satisfying two conditions:

- It decomposes into $\geq r$ mutually disjoint connected subgraphs;
- Each subgraph contains $\geq h + 1$ nodes.

Definition 4 [28]: In a system G, the h-extra r-component connectivity of G, denoted $\kappa_r^h(G)$, represents the minimum node cardinality among all possible h-extra r-component node cut in G.

Definition 5: In a system G, we say G satisfies h-extra r-component t-diagnosable if:

- $\forall F_1, F_2 \in \mathcal{F}_r^h(G)$ with $|F_1|, |F_2| \leq t$;
- (F_1, F_2) is a distinguishable pair.

The diagnosability number $\widehat{ec}_r^h(G)$ is the maximum value of t for which this condition holds.

III. Main Results

This section focuses on establishing the diagnosability of star graphs under two fault scenarios: (1) the 1-extra 2-component diagnosability; and (2) the 1-extra 3-component diagnosability.

In this context, we establish symbolic conventions for analyzing fault configurations in the n-dimensional star graph S_n ($n \geq 5$). Let $F \subseteq V(S_n)$ represent an arbitrary set of faulty nodes, with $F_\alpha = F \cap V(S_n^\alpha)$ denoting the restriction of these faults to the α-th coordinate subgraph for each $\alpha \in \langle n \rangle$. Based on the cardinality of F_α, we partition the coordinate set $\langle n \rangle$ into two disjoint subsets: $\mathbb{A} = \{\alpha \in \langle n \rangle \mid |F_\alpha| \geq n-2\}$, which aggregates coordinates where fault counts meet or exceed $n-2$, and its complement $\mathbb{B} = \langle n \rangle \setminus \mathbb{A}$, encompassing coordinates with fewer than $n-2$ faulty nodes. This partitioning facilitates subsequent analysis of fault distribution patterns across the star graph's structural components. Let $S_n^{\mathbb{A}}$ be the subgraph induced by $\cup_{\alpha \in \mathbb{A}} V(S_n^\alpha)$ and let $S_n^{\mathbb{B}}$ be the subgraph induced by $\cup_{\beta \in \mathbb{B}} V(S_n^\beta)$. Also, let $F_{\mathbb{A}} = \cup_{\alpha \in \mathbb{A}} F_\alpha$, and $F_{\mathbb{B}} = \cup_{\beta \in \mathbb{B}} F_\beta$. Let T be a connected component of the maximum cardinality in $G - F$. Then we refer to this component T is the large component, and all the other components of $G - F - V(T)$ as small components.

Lemma 3 [29]: In a star graph S_n with $n \geq 6$, consider a subset of faulty nodes F. If the size of F is bounded by $5n - 15$, the remaining graph $S_n - F$ retains connected subgraphs whose combined node count does not exceed four. Extending this, when F is limited to $6n - 19$ nodes, the total nodes across all intact functional segments in $S_n - F$ remain capped at five.

Lemma 4 [29]: For the n-dimensional star graph S_n, $\kappa_3^1(S_n) = 4n - 10$ when $n \geq 5$.

Lemma 5 [29]: For the n-dimensional star graph S_n, $\kappa_4^1(S_n) = 6n - 16$ when $n \geq 6$.

A. 1-Extra 2-Component Diagnosability of Star Graph

Lemma 6: The 1-extra 2-component diagnosability of S_n is $\widehat{ec}_2^1(S_n) \leq 4n - 9$ for $n \geq 5$.

Proof: Consider a set of four nodes $X = \{x_1, x_2, x_3, x_4\}$ in S_n, as illustrated in Fig. 2, where $(x_1, x_2), (x_3, x_4) \in E(S_n)$. Let $F_1 = N_{S_n}(X)$ and $F_2 = N_{S_n}(X) \cup \{x_3, x_4\}$. Assume that in S_n, nodes x_1 and x_3 share a common neighbor, x_2 and x_4 also share a common neighbor. First, we calculate $|N_{S_n}(X)|$,

$$|N_{S_n}(X)| = 4(n-3) + 2 = 4n - 10.$$

Thus, we have $|F_1| = 4n - 10 \leq 4n - 8$ and $|F_2| \leq 4n - 10 + 2 = 4n - 8$.

Next, we calculate the size of $\overline{F_1 \cup F_2} - \{x_1, x_2\}$,

$$\begin{aligned} &|V(S_n)| - |F_1 \cup F_2| - |X - \{x_3, x_4\}| \\ &= |V(S_n)| - |F_2| - |X - \{x_3, x_4\}| \\ &= n! - (4n-8) - 2 \end{aligned}$$

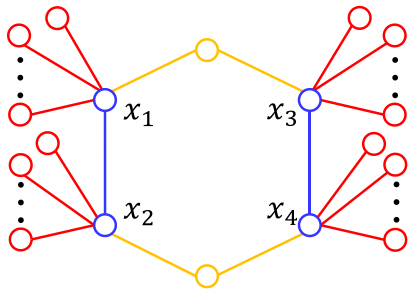

Fig. 2. Illustration of 1-extra 2-component cut.

$$\begin{aligned} &= n! - 4n + 6 \\ &\geq 2. \end{aligned}$$

Therefore, $S_n - F_1$ and $S_n - F_2$ contain multiple disconnected subgraphs, each with at least two nodes, indicating that both F_1 and F_2 are 1-extra 2-component cuts. Given that $F_1 \subset F_2$ and $F_1 \Delta F_2 = \{x_3, x_4\}$, there are no edges between $V(S_n) - (F_1 \cup F_2)$ and $F_1 \Delta F_2$, which indicates the indistinguishability of (F_1, F_2) under the PMC model.

Thus, we conclude that $\widehat{ec}_2^1(S_n) \leq 4n - 9$. □

Lemma 7. The 1-extra 2-component diagnosability of S_n is $\widehat{ec}_2^1(S_n) \geq 4n - 9$ for $n \geq 6$.

Proof: ssume, for the sake of contradiction, that $\widehat{ec}_2^1(S_n) \leq 4n - 10$. It means there exists an indistinguishable 1-extra 2-component node subset pair (F_1, F_2), where $|F_1| \leq 4n - 9$ and $|F_2| \leq 4n - 9$. W.l.o.g., assume $F_1 - F_2 \neq \emptyset$. According to Lemma 3, there exist a large component in $S_n - F_1$ with at least $|V(S_n) - F_1| - 4 = n! - (4n-9) - 4 = n! - 4n + 5$ nodes.

Let A be the union of the remaining small components in $S_n - F_1$, and B be the large component in $S_n - F_1$, i.e., $B = V(S_n) - F_1 - V(A)$. Therefore, we have

$$\begin{aligned} |V(B)| &= |V(S_n) - F_2 - V(A)| \\ &\geq n! - (4n-9) - 4 \\ &= n! - 4n + 5. \end{aligned}$$

Furthermore, $|V(B) - F_2| > 0$. Since F_1 and F_2 are indistinguishable in the PMC model, we have

$$E[V(B) \cap (F_2 - F_1), V(B) - (F_2 - F_1)] = \emptyset,$$

which means that $B \subseteq \overline{F_1 \cup F_2}$, and therefore, $V(B) \cap (F_2 - F_1) = \emptyset$. Since F_1 is a 1-extra 2-component cut in S_n, it follows that $F_2 - F_1$ is a subset of the small components in $S_n - F_1$, i.e., $F_2 - F_1 \subseteq V(A)$, and $|F_2 - F_1| \leq |V(A)| \leq 4$. As $E[V(A), V(B)] = \emptyset$ and $E[F_2 - F_1, V(B)] = \emptyset$, we conclude that B is a connected component of $S_n - (F_1 \cap F_2)$. We calculate

$$\begin{aligned} &|V(B) - V(A) - (F_1 - F_2)| \\ &\geq (n! - 4n + 5) - 4 - 4 \\ &= n! - 4n - 3 \\ &> 0 \end{aligned}$$

which means that B is the largest connected component in $S_n - (F_1 \cap F_2)$. The following discussion can be categorized into two scenarios based on the distribution of F_1, F_2 in S_n.

Case 1: $F_1 - F_2 \neq \emptyset$, $F_2 - F_1 \neq \emptyset$.

Given that F_1 is a 1-extra 2-component cut in S_n, both $|F_1 - F_2|$ and $|F_2 - F_1|$ are greater than or equal to two. Under the condition that $E[F_1, F_2] \neq \emptyset$ and $g(S_n) = 6$, the edge set $E[F_1, F_2]$ contains exactly one edge. This means that the neighborhood of $F_1 \Delta F_2$ satisfies $|N(F_1 \Delta F_2)| \geq 4n - 10$. Since $N(F_1 \Delta F_2) \subseteq F_1 \cap F_2$, it follows that $|F_1 \cap F_2| \geq 4n - 10$. However, the upper bound $|F_1 \cap F_2| \leq 4n - 11$ derived from the minimal disjoint subsets $|F_1 - F_2| \geq 2$ and $|F_2 - F_1| \geq 2$ leads to a contradiction, thereby negating this scenario. For another case where $E[F_1, F_2] = \emptyset$, the intersection $F_1 \cap F_2$ is a $\mathcal{F}_3^1(S_n)$. By Lemma 4, $|F_1 \cap F_2| \geq 4n - 10$, leading to $|F_1| = |F_1 - F_2| + |F_1 \cap F_2| \geq 4n - 10 + 2 = 4n - 8$, which directly contradicts the initial assumption.

Case 2: $F_1 - F_2 \neq \emptyset$, $F_2 - F_1 = \emptyset$.

Since F_2 is a 1-extra 2-component cut of S_n, $S_n - F_2$ contains at least two components. Since $F_1 - F_2$ has at least one component of size at least two, $S_n - F_1$ contains at least one large connected component B. Since F_1 is a 1-extra 2-component cut of S_n, $S_n - F_1$ contains at least two components. Thus, $S_n - F_2$ contains at least 3 components and at least two nodes in each component, i.e., F_2 is a $\mathcal{F}_3^1(S_n)$, so $|F_2| \geq \kappa_3^1(S_n) = 4n - 10$. The above gives $|F_1| = |F_1 - F_2| + |F_1 \cap F_2| \geq 2 + 4n - 10 = 4n - 8$, which contradicts the assumption.

In summary, $\widehat{ec}_2^1(S_n) \geq 4n - 9$. □

Theorem 1. The PMC model establishes $\widehat{ec}_2^1(S_n) = 4n - 9$ of S_n for $n \geq 6$.

B. 1-Extra 3-Component Diagnosability of Star Graph

Lemma 8: The 1-extra 3-component diagnosability of S_n is $\widehat{ec}_3^1(S_n) \leq 6n - 15$ for $n \geq 6$.

Proof: Consider a set of six nodes $X = \{x_1, x_2, x_3, x_4, x_5, x_6\}$ in S_n, as shown in Fig. 3, where the edges (x_1, x_2), (x_3, x_4), and $(x_5, x_6) \in E(S_n)$. Let $F_1 = N_{S_n}(X)$ and $F_2 = N_{S_n}(X) \cup \{x_5, x_6\}$. Consider the case where the nodes x_1, x_3 share a common neighbor, x_3, x_5 share a common neighbor, x_2, x_4 share a common neighbor, and x_4, x_6 share a common neighbor. Then, we calculate the size of the neighborhood of X,

$$|N_{S_n}(X)| = 4(n-3) + 2(n-4) + 4 = 6n - 16.$$

For F_1, $|F_1| = |N_{S_n}(X)| = 6n - 16 \leq 6n - 16 + 2 = 6n - 14$. Similarly, for F_2, the inclusion of nodes x_5, x_6 does not increase the upper bound beyond, $|F_2| = |F_1| + 2 \leq 6n - 16 + 2 = 6n - 14$.

Next, we calculate the size of the size of $\overline{F_1 \cup F_2} - \{x_1, x_2, x_3, x_4\}$,

$$\begin{aligned} &|V(S_n)| - |F_1 \cup F_2| - |X - \{x_5, x_6\}| \\ &= |V(S_n)| - |F_2| - |X - \{x_5, x_6\}| \\ &= n! - (6n - 14) + 2 \\ &\geq 2. \end{aligned}$$

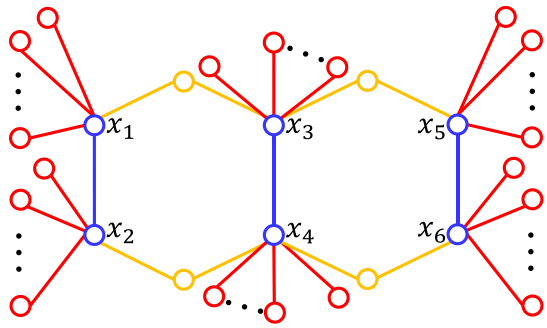

Fig. 3. Illustration of 1-extra 3-component cut.

Removing F_1 or F_2 will split S_n into three or more components, each containing at least two nodes, indicating that both F_1 and F_2 are $\mathcal{F}_3^1(S_n)$. Given $F_1 \subset F_2$ and $F_1 \Delta F_2 = \{x_5, x_6\}$, since there are no edges connecting $V(S_n) - (F_1 \cup F_2)$ and $F_1 \Delta F_2$, this proves that (F_1, F_2) is indistinguishable under the PMC model, leading to the conclusion that $\widehat{ec}_3^1(S_n) \leq 6n - 15$. □

Lemma 9: The 1-extra 3-component diagnosability of S_n is $\widehat{ec}_3^1(S_n) \geq 6n - 15$ for $n \geq 6$ under PMC model.

Proof: Suppose, for the sake of contradiction, that $\widehat{ec}_3^1(S_n) \leq 6n - 16$. This means there exists an indistinguishable 1-extra 3-component node subset pair (F_1, F_2), with $|F_1| \leq 6n - 15$ and $|F_2| \leq 6n - 15$. W.l.o.g., assume that $F_1 - F_2 \neq \emptyset$. Let S be a subset of $V(S_n)$. When $|S| = 7$, the neighborhood size is $|N_{S_n}(S)| \geq 5(n-3) + (n-4) + (n-2) = 7n - 21$. Thus, for $n \geq 6$, we have $6n - 15 \leq 7n - 22$. This means that there exists a large component in $S_n - F_1$ containing at least $|V(S_n) - F_1| - 6$ nodes. Let A be the union of the remaining small components in $S_n - F_1$, and B be the large component of $S_n - F_1$, i.e., $B = V(S_n) - F_1 - V(A)$. Then

$$\begin{aligned} |V(B)| &= |V(S_n) - F_2 - V(A)| \\ &\geq n! - (6n - 15) - 6 \\ &= n! - 6n + 9 \end{aligned}$$

In the PMC model, the indistinguishability of F_1 and F_2 means that there are no edges between $V(B) \cap (F_2 - F_1)$ and $V(B) \setminus (F_2 - F_1)$. Since B is connected and entirely contained within $\overline{F_1 \cup F_2}$, it cannot intersect with $F_2 - F_1$. Therefore, F_1 forms a $\mathcal{F}_3^1(S_n)$, and $F_2 - F_1$ lies within the component $V(A)$ of $S_n - F_1$, where $|F_2 - F_1| \leq |V(A)| \leq 6$. Therefore, there are no connecting edges between $V(A)$ and $V(B)$, nor between $F_2 - F_1$ and $V(B)$, which confirms that B is a connected component in $S_n - (F_1 \cap F_2)$.

Now, we consider

$$\begin{aligned} &|V(B) - V(A) - (F_1 - F_2)| \\ &\geq (n! - 6n + 9) - 6 - 6 \\ &= n! - 6n - 3 \\ &> 0, \end{aligned}$$

Therefore, B is the largest connected component of $S_n - (F_1 \cap F_2)$. This leads to two possible cases based on the distribution of F_1 and F_2 in S_n

Case 1: $F_1 - F_2 \neq \emptyset$, $F_2 - F_1 \neq \emptyset$.
Case 1.1: $A - (F_1 - F_2) \neq \emptyset$.

Since F_1 is a $\mathcal{F}_3^1(S_n)$, both $|F_1 - F_2|$ and $|F_2 - F_1|$ are greater than or equal to two. This ensures that $F_1 \cap F_2$ is a $\mathcal{F}_4^1(S_n)$. By applying Lemma 5, the lower bound $|F_1 \cap F_2| \geq 6n - 16$ leads to $|F_1| = |F_1 - F_2| + |F_1 \cap F_2| \geq 6n - 14$, which directly contradicts the initial assumption.

Case 1.2: $A - (F_1 - F_2) = \emptyset$.

Since F_1 is a $\mathcal{F}_3^1(S_n)$, both $|F_1 - F_2|$ and $|F_2 - F_1|$ are greater than or equal to four. Then, $F_1 \cap F_2$ is a $\mathcal{F}_4^1(S_n)$. By Lemma 5, $|F_1 \cap F_2| \geq 6n - 16$, resulting in $|F_1| = |F_1 - F_2| + |F_1 \cap F_2| \geq 6n - 14$, thereby contradicting the initial assumption.

Case 2: $F_1 - F_2 \neq \emptyset$, $F_2 - F_1 = \emptyset$.

Since F_2 is a $\mathcal{F}_3^1(S_n)$, $S_n - F_2$ contains at least two components. Among them, $F_1 - F_2$ has at least three components with a size no less than two, while $S_n - F_1$ contains at least one large connected component B. Since F_1 is a $\mathcal{F}_4^1(S_n)$, $S_n - F_1$ contains at least two components. Thus, $S_n - F_2$ contains at least three components and at least two nodes in each component, i.e., F_2 is a $\mathcal{F}_4^1(S_n)$, so $|F_2| \geq \kappa_4^1(S_n) = 6n - 16$. The above gives $|F_1| = |F_1 - F_2| + |F_1 \cap F_2| \geq 2 + 6n - 16 = 6n - 14$, which contradicts the assumption.

In summary, $\widehat{ec}_3^1(S_n) \geq 6n - 15$. □

Theorem 2: The PMC model establishes $\widehat{ec}_3^1(S_n) = 6n - 15$ as the 1-extra 3-component diagnosability of S_n for $n \geq 6$.

IV. Diagnostic Algorithm

As the complexity of interconnected networks increases, fault diagnosis becomes a key task for ensuring system stability and reliability. Traditional fault diagnosis algorithms often require extensive testing and long time delay, which leads to inefficiency and a high chance of misdiagnosis. To address this, we propose a fault diagnosis algorithm based on the trial system. This approach aims to improve the accuracy and efficiency of fault detection through a systematic process.

A. Algorithm Overview

The PMC simulation algorithm (Algorithm 1) introduced in this paper is a simulation implementation built based on the system-level diagnostic model PMC, aiming to simulate and generate a set of test symptoms. Compared to previous methods that use matrices to represent symptom sets, this work adopts a dictionary list format to store symptoms, significantly reducing the size of the symptom set and avoiding the sharp increase in time complexity caused by matrix traversal in subsequent diagnostic algorithms. This achieves an optimization of the symptom set size from exponential to linear level. The inputs of this algorithm include a graph G and a preset faulty node set $faulty\_nodes$ (note that the faulty node set here is preset for experimental simulation purposes; in practical applications, the distribution and number of faulty nodes are usually unknown and may require tools such as the ping command for testing). The algorithm process is as follows: First, each node u in G is traversed, and each neighbor node v can be tested. The testing logic is determined based on the faulty status of node u and randomness rules: (1) If node u is faulty, it decides randomly whether to record neighbor node v as a value of u; (2) If node u is not faulty but its neighbor node v is faulty, v is directly recorded as a value of u.

This process stores symptom information through a dictionary (structured in $key : value$ format, where the key represents the test node u, and the value is a list of neighbor nodes tested as 1 (i.e., faulty) by u). After traversing all neighbors of node u, if its symptom list $u.values$ is non-empty, the corresponding entry $u : u.values$ is added to the symptom set sym. Finally, the algorithm outputs the sym set, which contains information on all test nodes in the graph and their corresponding neighbor nodes tested as 1 (faulty).

Next, here is a detailed introduction to our Trial System-based Fault Diagnosis Algorithm (TSFD) (Algorithm 2), which is deeply inspired by the process of the trial system. An overview of the specific process is as follows:

- **Plaintiff:** Fault-free nodes that represent the normal operating state of the system.
- **Defendant:** Faulty nodes that may lead to system failure.
- **Investigation Method:** The PMC model, used to model the relationship between symptoms and faults in the system.
- **Evidence:** A dictionary of symptoms obtained by PMC.

Next, we will provide a detailed explanation of our algorithm process (see Fig. 4).

1) **Presentation of Evidence (Algorithm 1):** First, we test through the PMC model to get the symptom dictionary. For example, node A has four neighbors B, C, D, and E, where C and D are the fauly node (here is the assumption, in practice, it is implemented in a manner similar to ping), then $\sigma(A, C) = 1$, $\sigma(A, D) = 1$ through the PMC model test. Next, we add C and D to the value of A to form A's symptom dictionary like $\{A : C, D\}$.
2) **Plaintiff's Statement (Algorithm 2 [Lines 1-6]):** The algorithm scans the symptom dictionary and adds all values to $doubt\_list$(the list of doubted faulty nodes).
3) **Defendant's Response (Algorithm 2 [Lines 7-10]):** Checking is conducted on the nodes in the suspected faulty node list. Assume that the test result for node D is accurate, for node B is inaccurate.
4) **Trial (Algorithm 2 [Lines 11-12]):** Based on the test results, the algorithm removes nodes with accurate test results (node D) from the suspected faulty node list, leaving node B.
5) **Verdict (Algorithm 2 [Lines 13-15]):** Finally, the output list of faulty nodes is $[B, E, C, F]$, indicating these nodes are determined to be a faulty node.

B. Performance Analysis

Next, we analyze the performance of the algorithm. In addition, to better validate the performance of the algorithm, we design and conduct simulation experiments. These experiments evaluate the algorithm's performance in the star network.

1) Time Complexity Analysis: The first step is to calculate its time complexity. It is important to note that Algorithm 1 is

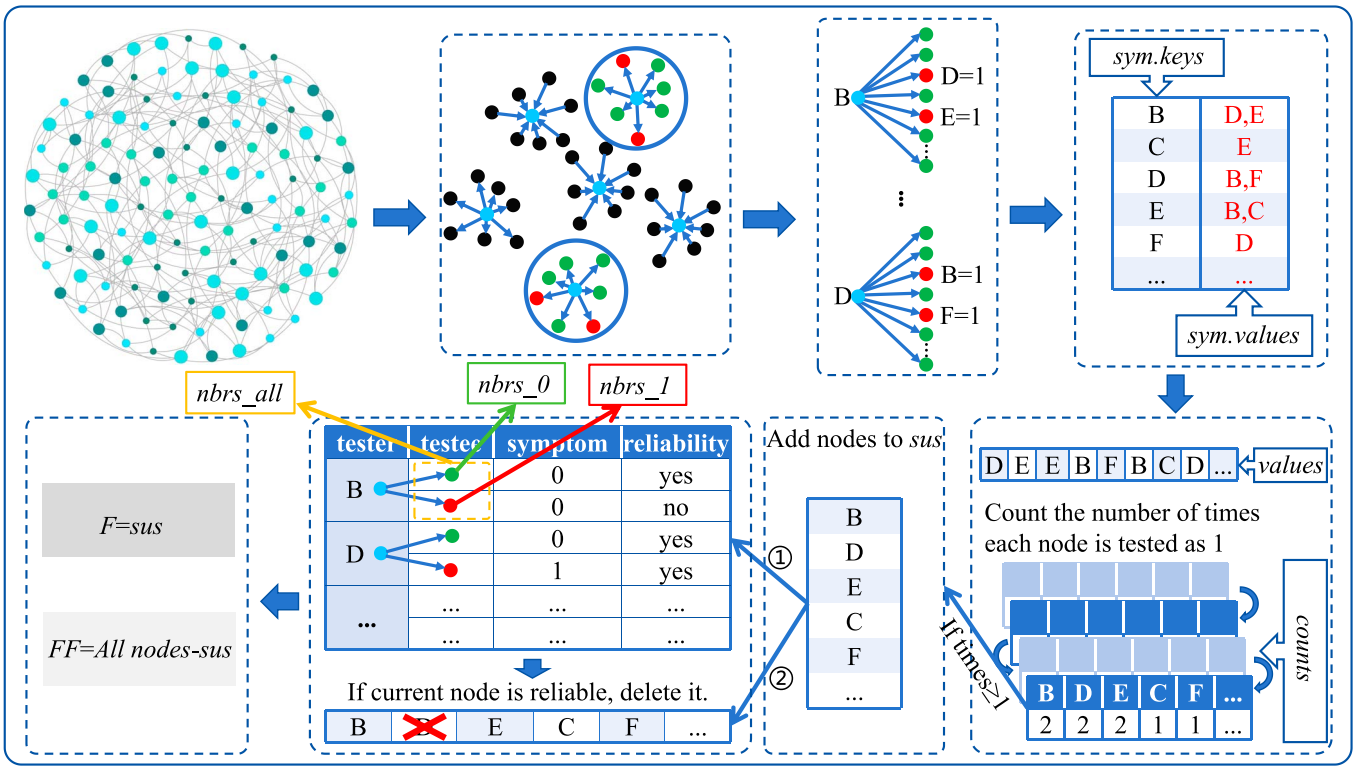

Fig. 4. Algorithm process.

Algorithm 1: Simulation Algorithm of PMC.

Input: G: Graph, $faulty\_nodes$: Set of faulty nodes
Output: sym: Set of test symptom

$sym \leftarrow \{\}$;
for *each node* u ***in*** G **do**
  $u.values \leftarrow []$;
  for *each node* v ***in*** G ***and*** (u, v) *is an edge* **do**
    if u *in* $faulty\_nodes$ **then**
      if *Random choice* $\in \{0, 1\}$ *is* 1 **then**
        add v **as the value of** u ;
    else
      if v *in* $faulty\_nodes$ **then**
        add v **as the value of** u ;
  if $u.values! = \emptyset$ **then**
    $sym.append\{u : u.values\}$;
return sym ;

not the main focus of this paper, so we do not analyze it in detail. Our focus is on calculating the time complexity of Algorithm 2.

Theorem 3: The time complexity of the TSFD Algorithm is expressed as $O(Nd)$, where N signifies the total nodes in the system G, d denotes the uniform degree of its regular structure, and Γ represents the quantity of faulty nodes.

Proof: The time taken to execute one stage of the TSFD algorithm is listed below.

- **Step 1** Initialization: $O(1)$;
- **Steps 2-3** Collect all symptom-related nodes: $O(Nd)$;
- **Step 4** Count Node Frequencies: $O(\Gamma)$;
- **Steps 5-6** Filter Suspicious Nodes: $O(\Gamma)$;
- **Steps 7-12** Second Filtering: $O(d\Gamma)$;
- **Steps 13-14** Update Fault and Fault-Free Lists: $O(1)$;
- **Step 15** Return Results: $O(1)$.

Therefore, the time complexity of the TSFD algorithm is $O(1) + O(Nd) + O(\Gamma) + O(d\Gamma) = O(Nd)$. □

Compared to existing mainstream solutions, the proposed algorithm demonstrates significant advantages in time efficiency. Specifically, the algorithm proposed by [30] has a complexity of $O(t^2\theta N)$, whose performance is simultaneously affected by the system's maximum fault size t and the network's maximum degree θ. The solution by [31] reduces the complexity to $O(t^2 N)$, decreasing its dependence on node degrees, but it still remains proportional to t^2 in the worst-case scenario. For large-scale systems, the quadratic term t^2 incurs substantial overhead. The approach by [32] achieves a complexity of $O(N(\log_2 N)^2)$, exhibiting a near-linear growth trend, yet it is still influenced by the logarithmic squared term. In contrast, the complexity of our algorithm, $O(Nd)$, is strictly linear, scaling only with the system size N and a constant d. In regular interconnection networks (such as hypercubes, star graphs, etc.), d is a constant significantly smaller than N, and typically $d \leq \theta$. Therefore, our algorithm not only eliminates dependence on unpredictable fault size t, but its linear scaling property also outperforms existing sublinear and quadratic complexity solutions, with particularly notable efficiency improvements in large-scale network

Algorithm 2: Trial System-based Fault Diagnosis Algorithm (TSFD).

Input: G: Graph, sym: Symptom dictionary
Output: F: Faulty nodes, FF:Fault-Free nodes

$list\_1 \leftarrow [\,], FF \leftarrow [\,], F \leftarrow [\,]$;
for *each node* ***in*** $sym.values()$ **do**
  $list\_1.add(node)$; /*Collect the values in the symptom dictionary*/
Count the number of times each node appears in $list\_1$ and save them to $counts\_list$ in the form of $\{node : frequency\}$;
for *each node* ***in*** $counts\_list$ **do**
  $doubt\_list.add(node)$; /*Collect a list of doubted faulty nodes*/
for *each* sus_node ***in*** $doubt\_list$ **do**
  $nbrs\_all \leftarrow sus\_node.getNeighbors()$; /*Get all neighbors of node sus_node*/
  $nbrs\_1 \leftarrow sym.get(sus\_node)$; /*Get values of node sus_node in sym*/
  $nbrs\_0 \leftarrow nbrs\_all - nbrs\_1$;
  if $nbrs\_1.allNodes()$ *are in* $doubt\_list$ ***and*** $nbrs\_0.allNodes()$ *are not in* $doubt\_list$ **then**
    $doubt\_list.remove(sus\_node)$;
$F \leftarrow doubt\_list$;
$FF \leftarrow G.nodes() - F$;
return F, FF ;

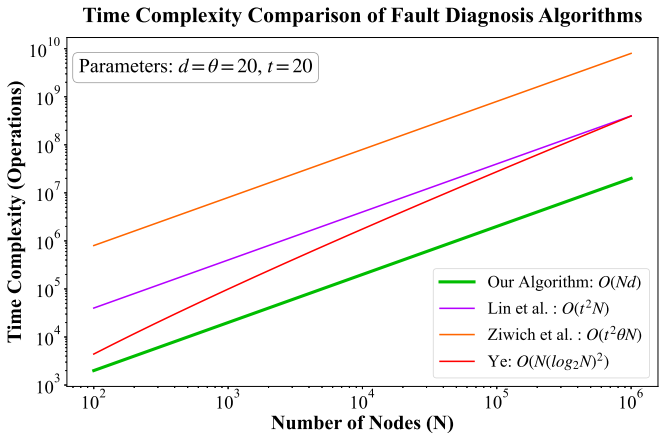

Fig. 5. Time complexity comparison of fault diagnosis algorithms.

environments (The comparison of time complexity is detailed in Fig. 5).

2) Simulation Experiments: To evaluate the performance of our algorithm more deeply, we execute simulation experiments. Before introducing these experiments in detail, first introduce some key performance evaluation metrics to measure the algorithm's effectiveness more accurately.

- **Accuracy:** $Accuracy = \frac{TP+TN}{TP+TN+FP+FN}$
- **Precision:** $Precision = \frac{TP}{TP+FP}$
- **Recall (TPR):** $Recall/TPR = \frac{TP}{TP+FN}$

TABLE I
EXPERIMENTAL SETUP

Name	Specification
CPU	AMD Ryzen 7 4700G
Memory	32 GB DDR4
Operating System	Windows 11
Programming Language	Python 3.8
Key Library	NetworkX

- **F1 Score:** $F1 = 2 * \frac{Precision*Recall}{Precision+Recal}$
- **FPR:** $FPR = \frac{FP}{FP+TN}$
- **TNR:** $TNR = \frac{TN}{FP+TN}$
- **FNR:** $FNR = \frac{FN}{TP+FN}$
- **G-Mean:** $G\text{-}Mean = \sqrt{Recall * Precision}$

In diagnostic systems, True Positives (TP) represent the number of actually faulty nodes correctly identified as faulty, while True Negatives (TN) correspond to the count of genuinely healthy nodes accurately classified as fault-free; False Positives (FP) denote the misclassification of fault-free nodes as faulty (over-reporting), and False Negatives (FN) reflect the failure to detect truly faulty nodes or their erroneous categorization as healthy (under-reporting). These four metrics collectively quantify the precision and reliability of the diagnostic mechanism. The selection of the above evaluation metrics stems from the need to comprehensively assess the performance of our fault diagnosis method in typical class-imbalanced scenarios of interconnected networks, where faulty nodes are usually far fewer than normal nodes. Each metric provides a unique perspective. Accuracy, precision, recall, and F1-score reflect classification performance from multiple dimensions, emphasizing the trade-off between detecting true faults and minimizing false alarms. The FPR, TNR, and FNR offer critical insights into error types, particularly crucial for evaluating false alarms (FPR) and missed detections (FNR), which are decisive in fault-tolerant systems. The geometric mean is especially important in class-imbalanced scenarios, as it balances sensitivity (Recall) and specificity (TNR), preventing model performance from being biased toward the majority class. Together, these metrics ensure a rigorous evaluation of diagnostic reliability and robustness.

In the simulation experiment, we first generate star graphs of different dimensions ($n = 6, 7, 8$), forming the baselined dataset. Refer to Table I for the experimental setup. Taking $n = 6$ as an example, we preset the fault node counts as $(19, 32, 46, 60, 74, 88, 102, 116, 130, 144)$, while their specific locations are randomly generated in each experiment to simulate the uncertainty of real-network. Each generated graph G and its corresponding faulty nodes are input into Algorithm 1 to perform the PMC testing. This step yields the symptom sets caused by faults, which are then fed into the TSFD algorithm for diagnosis. The TSFD algorithm operates in a "blind" state, unaware of the fault node count or distribution, relying solely on the symptom set for reasoning. The diagnosis results are compared with the actual fault nodes to evaluate performance using metrics such as Accuracy, Recall, and F1-score. To ensure reliability, 1000 repeated experiments are conducted for

TABLE II
PERFORMANCE OF TSFD IN S_6

Number of Fault Nodes	19	32	46	60	74	88	102	116	130	144
Accuracy	0.9992	0.9986	0.9979	0.9972	0.9964	0.9955	0.9945	0.9932	0.9916	0.9899
Precision	0.9692	0.9685	0.9683	0.9675	0.9661	0.9654	0.9635	0.9613	0.9575	0.9544
Recall	0.9998	0.9998	0.9995	0.999	0.9988	0.998	0.9976	0.9967	0.9958	0.995
F1 Score	0.9839	0.9836	0.9835	0.9829	0.9821	0.9813	0.9802	0.9786	0.9762	0.9742
G-Mean	0.9995	0.9992	0.9987	0.998	0.9975	0.9966	0.9958	0.9946	0.9932	0.9918
FPR	0.0008	0.0015	0.0022	0.0029	0.0039	0.0048	0.006	0.0074	0.0093	0.0113
TNR	0.9992	0.9985	0.9978	0.9971	0.9961	0.9952	0.994	0.9926	0.9907	0.9887
FNR	0.0002	0.0002	0.0005	0.001	0.0012	0.002	0.0024	0.0033	0.0042	0.005

TABLE III
PERFORMANCE OF TSFD IN S_7

Number of Fault Nodes	25	134	243	352	461	571	680	789	898	1008
Accuracy	0.9999	0.9996	0.9992	0.9988	0.9984	0.9978	0.9971	0.9962	0.9949	0.9934
Precision	0.9852	0.9843	0.9842	0.9833	0.9826	0.9808	0.9785	0.9759	0.9718	0.9673
Recall	1	1	1	1	0.9999	0.9999	0.9998	0.9997	0.9996	0.9994
F1 Score	0.9924	0.9921	0.992	0.9916	0.9912	0.9902	0.9891	0.9877	0.9855	0.9831
G-Mean	1	0.9998	0.9996	0.9994	0.9991	0.9987	0.9982	0.9976	0.9968	0.9957
FPR	0.0001	0.0004	0.0008	0.0013	0.0018	0.0024	0.0033	0.0044	0.0061	0.0081
TNR	0.9999	0.9996	0.9992	0.9987	0.9982	0.9976	0.9967	0.9956	0.9939	0.9919
FNR	0	0	0	0	0.0001	0.0001	0.0002	0.0003	0.0004	0.0006

TABLE IV
PERFORMANCE OF TSFD IN S_8

Number of Fault Nodes	31	923	1816	2708	3601	4493	5386	6278	7171	8064
Accuracy	1	0.9998	0.9996	0.9994	0.999	0.9985	0.9978	0.9967	0.9952	0.9931
Precision	0.9934	0.9922	0.9918	0.9909	0.9893	0.9869	0.9835	0.9789	0.9728	0.9657
Recall	1	1	1	1	1	1	1	1	0.9999	0.9999
F1 Score	0.9966	0.9961	0.9959	0.9954	0.9946	0.9934	0.9917	0.9893	0.9862	0.9825
G-Mean	1	0.9999	0.9998	0.9997	0.9995	0.9992	0.9987	0.998	0.997	0.9957
FPR	0	0.0002	0.0004	0.0007	0.001	0.0016	0.0025	0.0039	0.0058	0.0085
TNR	1	0.9998	0.9996	0.9993	0.999	0.9984	0.9975	0.9961	0.9942	0.9915
FNR	0	0	0	0	0	0	0	0	0.0001	0.0001

each dimension. This repetition reduces randomness bias and provides stable results.

Finally, the average values of key metrics are computed in these 1000 repeated experiments to assess the stability, robustness, and overall effectiveness of the TSFD algorithm under different conditions. The averages of these experiments constitute the final experimental results.

Tables II–IV show that TSFD has a high performance in S_6, S_7 and S_8. The performance analysis of TSFD on star graphs S_6, S_7, and S_8 demonstrates its stability and effectiveness at varying fault levels. As the number of faulty nodes increases, Accuracy shows a slight decrease, with S_6 dropping from 0.9992 to 0.9899, S_7 from 0.9999 to 0.9934, and S_8 from 1 to 0.9931. Precision remains consistently above 95% for all graphs, indicating reliable fault detection, although it slightly decreases due to an increase in FPR. Recall remains exceptionally high, staying above 0.995 for S_6, 0.9994 for S_7, and near 1 for S_8, confirming strong fault coverage.

The F1 score, which balances precision and recall, reflects stable performance, with values above 0.97 across all graphs. Similarly, the G-Mean stays high, indicating minimal impact on overall classification accuracy. While the false positive rate (FPR) and false negative rate (FNR) increase slightly as the fault density grows, the changes remain small, showing that TSFD continues to effectively identify most faulty nodes and avoids significant misclassifications of non-faulty nodes.

Overall, the results confirm that TSFD maintains high and stable performance across S_6, S_7, and S_8, even as the number of faulty nodes increases. This demonstrates its robustness and reliability in handling faults in star graph structures.

Next we compare diagnostic strategies on star graph, including t/k-diagnosability ($k = 1, 2, 3$, Zhou et al. [33]), $\{1, 2\}$-extra diagnosability (Lv et al. [34]), $\{2, 3\}$-component diagnosability (Wan et al. [35]), and our proposed 1-extra $\{2, 3\}$-component diagnosability. As shown in Fig. 6, in the comparison of network diagnosability for Star Graphs, the data clearly demonstrates that 1-extra 2-component diagnosability and 1-extra 3-component diagnosability significantly outperform traditional and other enhanced diagnostic strategies in fault-tolerant diagnostic capability. As the network dimension (n) increases, these two metrics consistently exhibit the highest diagnostic values, highlighting their superior performance. For instance, when $n = 24$, the 1-extra 2-component diagnosability reaches 87, while the 1-extra 3-component diagnosability reaches as high as 129, far exceeding other strategies such as t/1-diagnosability or 2-component diagnosability. This

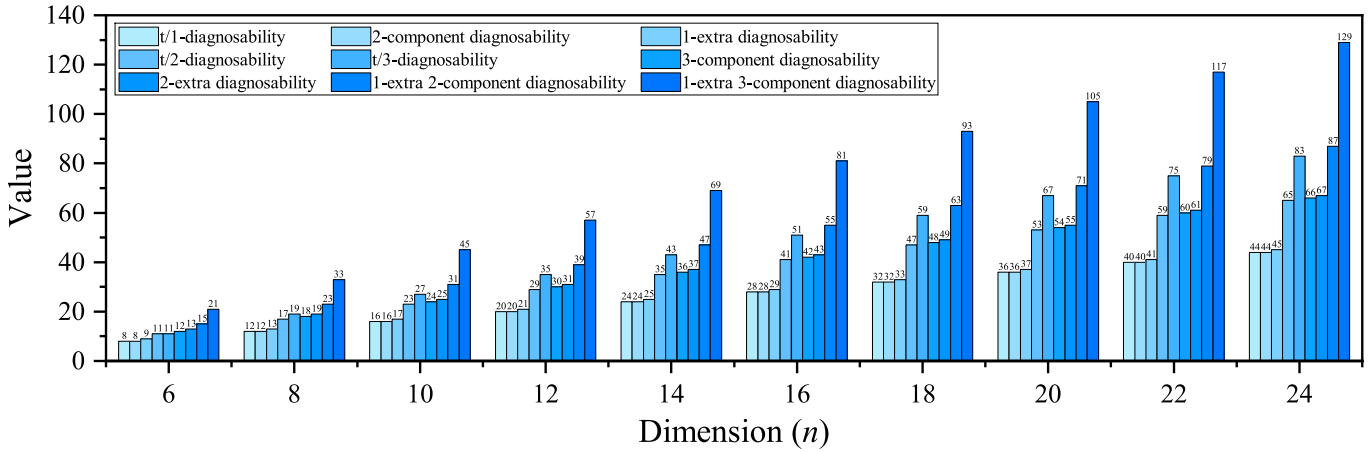

Fig. 6. The performance of different diagnostic strategies in $S_n(6 \leq n \leq 24)$.

advantage stems from their combination of additional fault tolerance and multi-component fault diagnosis capabilities, granting them stronger system-level diagnostic reliability and robustness in complex fault scenarios.

3) Application experiment of TSFD fault diagnosis algorithm in data center network $BCube$: This experiment aims to evaluate the performance of our proposed algorithm in the BCube network architecture of data centers. BCube is a high-performance network topology specifically designed for data centers, featuring a recursive structure where $BCube(n, k)$ represents a network with $k+1$ layers, each containing n^k n-port switches, and a total of n^{k+1} servers. This structure offers excellent fault tolerance and scalability, making it widely adopted in modern data centers.

The experiment first constructed BCube networks of varying scales—specifically, $n = 10, 11, 12, 13$ with $k = 3$—resulting in node counts of 10,000, 14,641, 20,736, and 28,561, respectively. In each network, varying numbers of faults (ranging from 0 to approximately 2,000-5,700) are incrementally injected, and the TSFD fault diagnosis algorithm was deployed to identify node states. To ensure statistical reliability, each experiment was repeated 1,000 times, with final metrics averaged.

The results (Table V) demonstrate that the TSFD algorithm exhibits exceptionally high accuracy and stability in BCube networks. Specifically, across all test cases, precision remained consistently at 1, indicating no false alarms and outstanding reliability. As the number of faulty nodes increased, recall gradually declined but remained at a high level. For instance, even under the maximum tested fault load (e.g., 2,000 faults in $BCube(10, 3)$), Recall still reached 0.8161, with the F1-score maintaining 0.8987, demonstrating the algorithm's robust identification capability in large-scale fault scenarios. Additionally, the geometric mean (G-Mean) trend aligned with the F1-Score, further validating the algorithm's balanced performance across different classes.

In summary, the TSFD algorithm performs excellently across various BCube scales and fault scenarios, particularly excelling

TABLE V
PERFORMANCE EVALUATION RESULTS OF BCUBE(n, k), WHERE $n = 10, 11, 12, 13, k = 3$

Graph	Nodes	Faults	Accuracy	Precision	Recall	F1-Score	G-Mean	FNR
BCube(10,3)	10000	0	1.0000	0.0000	0.0000	0.0000	0.0000	0.0000
		222	1.0000	1.0000	1.0000	1.0000	1.0000	0.0000
		444	1.0000	1.0000	1.0000	1.0000	1.0000	0.0000
		666	1.0000	1.0000	0.9999	1.0000	1.0000	0.0001
		888	0.9999	1.0000	0.9990	0.9995	0.9995	0.0010
		1111	0.9994	1.0000	0.9943	0.9971	0.9971	0.0057
		1333	0.9969	1.0000	0.9776	0.9887	0.9887	0.0224
		1555	0.9904	1.0000	0.9422	0.9702	0.9706	0.0578
		1777	0.9770	1.0000	0.8853	0.9391	0.9409	0.1147
		2000	0.9549	1.0000	0.8161	0.8987	0.9034	0.1840
BCube(11,3)	14641	0	1.0000	0.0000	0.0000	0.0000	0.0000	0.0000
		325	1.0000	1.0000	1.0000	1.0000	1.0000	0.0000
		650	1.0000	1.0000	1.0000	1.0000	1.0000	0.0000
		976	1.0000	1.0000	1.0000	1.0000	1.0000	0.0000
		1301	1.0000	1.0000	0.9997	0.9999	0.9999	0.0003
		1626	0.9998	1.0000	0.9986	0.9993	0.9993	0.0014
		1952	0.9990	1.0000	0.9923	0.9961	0.9961	0.0077
		2277	0.9959	1.0000	0.9742	0.9869	0.9870	0.0258
		2602	0.9877	1.0000	0.9352	0.9665	0.9670	0.0648
		2928	0.9724	1.0000	0.8787	0.9354	0.9374	0.1213
BCube(12,3)	20736	0	1.0000	0.0000	0.0000	0.0000	0.0000	0.0000
		460	1.0000	1.0000	1.0000	1.0000	1.0000	0.0000
		921	1.0000	1.0000	1.0000	1.0000	1.0000	0.0000
		1382	1.0000	1.0000	1.0000	1.0000	1.0000	0.0000
		1843	1.0000	1.0000	0.9999	1.0000	1.0000	0.0001
		2303	1.0000	1.0000	0.9997	0.9998	0.9998	0.0003
		2764	0.9997	1.0000	0.9975	0.9988	0.9988	0.0025
		3225	0.9982	1.0000	0.9885	0.9942	0.9942	0.0115
		3686	0.9936	1.0000	0.9654	0.9824	0.9825	0.0346
		4147	0.9834	1.0000	0.9233	0.9601	0.9609	0.0767
BCube(13,3)	28561	0	1.0000	0.0000	0.0000	0.0000	0.0000	0.0000
		634	1.0000	1.0000	1.0000	1.0000	1.0000	0.0000
		1269	1.0000	1.0000	1.0000	1.0000	1.0000	0.0000
		1904	1.0000	1.0000	1.0000	1.0000	1.0000	0.0000
		2538	1.0000	1.0000	1.0000	1.0000	1.0000	0.0000
		3173	1.0000	1.0000	0.9999	0.9999	0.9999	0.0001
		3808	0.9999	1.0000	0.9993	0.9996	0.9996	0.0007
		4442	0.9992	1.0000	0.9951	0.9975	0.9975	0.0049
		5077	0.9968	1.0000	0.9824	0.9911	0.9912	0.0176
		5712	0.9901	1.0000	0.9527	0.9758	0.9761	0.0473

in low false positives and high precision, proving its effectiveness and robustness in real-world data center network fault diagnosis.

V. Discussion and Application

A. Discussion on the Universality of TSFD Fault Diagnosis Algorithm

The TSFD fault diagnosis algorithm proposed in this paper is not only suitable for star networks but can also be applied to other network topologies. The algorithm uses the PMC model for initial testing to collect symptom information. It then employs a two-step diagnostic mechanism, including forward reasoning and backward exclusion, to accurately identify faulty nodes and significantly reduce misdiagnosis. Since the core process relies only on the relationships between nodes and edges in the graph and does not impose specific constraints on the topology, the algorithm can be extended to any graph where edges have no directions and every edge has two distinct end nodes. However, it should be noted that different topologies, such as mesh, tree, or hierarchical structures, may have varying connectivity and fault propagation characteristics. These differences could influence diagnostic accuracy. Therefore, we will systematically evaluate the performance of the TSFD algorithm in various network structures in future work to further verify and optimize its general applicability.

B. Discussion on the Practical Deployment Issues of TSFD Fault Diagnosis Algorithm

In engineering practice, the characteristics of the Star Graph make it particularly suitable for structured topology scenarios such as high-performance computing clusters, distributed storage systems, and data center networks. Against this backdrop, the TSFD fault diagnosis algorithm proposed in this study can be deployed in a distributed architecture: the core algorithm runs on a dedicated diagnostic server, while a PMC testing program is embedded in each computing node. These programs periodically perform self-checks and aggregate symptom data to the diagnostic server. Leveraging the TSFD algorithm, the server conducts collaborative analysis and probabilistic reasoning on multi-source data, enabling rapid localization and diagnosis of node faults. This architecture boasts excellent scalability, as new nodes can be integrated into the diagnostic scope simply by incorporating a PMC testing program. To address heterogeneous devices and multi-protocol environments, unified testing standards can be established to ensure compatibility. Additionally, the system incorporates a threshold-based real-time alerting and log analysis mechanism for continuous monitoring of diagnostic performance.

C. Discussion on the Fault Diagnosis Problem of TSFD Fault Diagnosis Algorithm Under Dynamic Environments

This study currently focuses on theoretical analysis and validation under static fault scenarios, which, while foundational for evaluating the performance of h-extra r-component diagnosability, also acknowledges the necessity of extending the research to dynamic environments. From a theoretical framework perspective, the TSFD algorithm proposed in this paper is inherently a diagnostic framework based on periodic testing and symptom analysis, possessing the potential to handle dynamic faults. By setting a reasonable diagnostic interval (T), the system can periodically collect symptom information and execute the algorithm, thereby continuously "capturing" system state snapshots, identifying newly occurring faults, and updating the set of faulty components to achieve near real-time tracking of fault evolution.

VI. Concluding Remarks

In this work, we investigate the h-extra r-component diagnosability of star graphs under the PMC model, providing both theoretical proofs and practical diagnosis algorithm. We derive results for $\widehat{ec}_2^1(S_n)$ and $\widehat{ec}_3^1(S_n)$. Furthermore, we propose the Fault Diagnosis Algorithm based on Trial System (TSFD), which leverages systematic diagnosis principles inspired by trial processes. Our experimental results affirm the algorithm's robustness, accuracy, and efficiency across various fault scenarios. This study enhances the understanding of network resilience and fault diagnosis in star graphs, offering a novel metric for evaluating diagnosability under complex fault conditions.

Future research will expand on this work by exploring the applicability of $\widehat{ec}_r^h(G)$ in other network topologies (such as hypercubes or mesh networks) and gradually increasing the value ranges of h and r, further optimizing the diagnostic process through the integration of machine learning techniques. Additionally, extending the algorithm to address dynamic fault scenarios significantly enhances its applicability to modern, evolving network architectures.

References

[1] S. Akers and B. Krishnamurthy, "A group-theoretic model for symmetric interconnection networks," *IEEE Trans. Comput.*, vol. 38, no. 4, pp. 555–566, Apr. 1989, doi: 10.1109/12.21148.

[2] F. P. Preparata, G. Metze, and R. T. Chien, "On the connection assignment problem of diagnosable systems," *IEEE Trans. Electron. Comput.*, vol. EC-16, no. 6, pp. 848–854, Dec. 1967, doi: 10.1109/PGEC.1967.264748.

[3] E. Cheng, L. Lipták, K. Qiu, and Z. Shen, "A unified approach to the conditional diagnosability of interconnection networks," *J. Interconnect. Netw.*, vol. 13, 2012, Art. no. 1250007, doi: 10.1142/S0219265912500077.

[4] S. Zhang and W. Yang, "The g-extra conditional diagnosability and sequential t/k-diagnosability of hypercubes," *Int. J. Computer Math.*, vol. 93, no. 3, pp. 482–497, Mar. 2016, doi: 10.1080/00207160.2015.1020796.

[5] L. Li, X. Zhang, Q. Zhu, and Y. Bai, "The 3-extra conditional diagnosability of balanced hypercubes under MM$*$ model," *Discrete Appl. Math.*, vol. 309, pp. 310–316, Mar. 2022, doi: 10.1016/j.dam.2021.04.004.

[6] W. Zheng, S. Zhou, E. Cheng, and Q. Zhang, "Non-inclusive g-extra diagnosability of interconnection networks under PMC model," *Theor. Computer Sci.*, vol. 1022, 2024, Art. no. 114887, doi: 10.1016/j.tcs.2024.114887.

[7] E. Cheng and L. Lipták, "Linearly many faults in Cayley graphs generated by transposition trees," *Inf. Sci.*, vol. 177, no. 22, pp. 4877–4882, Nov. 2007, doi: 10.1016/j.ins.2007.05.034.

[8] E. Cheng and L. Lipták, "Fault resiliency of Cayley graphs generated by transpositions," *Int. J. Foundations Computer Sci.*, vol. 18, no. 5, pp. 1005–1022, Nov. 2011, doi: 10.1142/S0129054107005108.

[9] L. Lin, L. Xu, S. Zhou, and S.-Y. Hsieh, "The t/k-diagnosability for regular networks," *IEEE Trans. Comput.*, vol. 65, no. 10, pp. 3157–3170, Oct. 2016, doi: 10.1109/tc.2015.2512866.
[10] L. Lin, Y. Huang, D. Wang, S. Y. Hsieh, and L. Xu, "A novel measurement for network reliability," *IEEE Trans. Comput.*, vol. 70, no. 10, pp. 1719–1731, Oct. 2021, doi: 10.1109/TC.2020.3023120.
[11] Y. Tian, Q. Zhu, and C. Lv, "Extra conditional diagnosability of hypercubes under the Bounded PMC model," in *Proc. Asia Conf. Algorithms, Comput. Mach. Learn. (CACML)*, 2022, pp. 391–396, doi: 10.1109/CACML55074.2022.00072.
[12] S. Zhang, D. Liang, L. Chen, R. Li, and W. Yang, "The component diagnosability of hypercubes with large-scale faulty nodes," *Comput. J.*, vol. 65, no. 5, pp. 1129–1143, May 2022, doi: 10.1093/comjnl/bxaa155.
[13] H. Zhuang, W. Guo, X. Li, X. Liu, and C.-K. Lin, "The component diagnosability of general networks," *Int. J. Foundations Comput. Sci.*, vol. 33, no. 1, pp. 67–89, Jan. 2022, doi: 10.1142/s0129054121500374.
[14] H. Zhuang, W. Guo, X.-Y. Li, X. Liu, and C.-K. Lin, "The component connectivity, component diagnosability, and t/k-diagnosability of Bicube networks," *Theor. Comput. Sci.*, vol. 896, pp. 145–157, Dec. 2021, doi: 10.1016/j.tcs.2021.10.011.
[15] Y. Huang, K. Wen, L. Lin, L. Xu, and S.-Y. Hsieh, "Component fault diagnosability of hierarchical cubic networks," *ACM Trans. Des. Autom. Electron. Syst.*, vol. 28, no. 3, pp. 1–19, May 2023, doi: 10.1145/3577018.
[16] J. Liu, S. Zhou, D. Wang, and H. Zhang, "Component diagnosability in terms of component connectivity of hypercube-based compound networks," *J. Parallel Distrib. Comput.*, vol. 162, pp. 17–26, Apr. 2022, doi: 10.1016/j.jpdc.2021.12.004.
[17] Y. Tian and Q. Zhu, "R-component diagnosability of hypercubes under the PMC model," *Theor. Comput. Sci.*, vol. 933, pp. 114–124, Oct. 2022, doi: 10.1016/j.tcs.2022.08.026.
[18] S.-L. Peng, C.-K. Lin, J. J. M. Tan, and L.-H. Hsu, "The g-good-neighbor conditional diagnosability of hypercube under PMC model," *Appl. Math. Comput.*, vol. 218, no. 21, pp. 10406–10412, Jul. 2012, doi: 10.1016/j.amc.2012.03.092.
[19] W. Fan, F. Xiao, H. Cai, X. Chen, and S. Yu, "Disjoint paths construction and fault-tolerant routing in BCube of data center networks," *IEEE Trans. Comput.*, vol. 72, no. 9, pp. 2467–2481, Sep. 2023, doi: 10.1109/TC.2023.3251849.
[20] W. Lin, X.-Y. Li, J.-M. Chang, and X. Jia, "Constructing multiple CISTs on BCube-based data center networks in the occurrence of switch failures," *IEEE Trans. Comput.*, vol. 72, no. 7, pp. 1971–1984, Jul. 2023, doi: 10.1109/TC.2022.3230288.
[21] H. Zhang, S. Zhou, E. Cheng, and S.-Y. Hsieh, "Characterization of cyclic diagnosability of regular diagnosable networks," *IEEE Trans. Rel.*, vol. 73, no. 1, pp. 270–278, Mar. 2024, doi: 10.1109/TR.2023.3301542.
[22] Y. Huang, L. Lin, L. Xu, and S.-Y. Hsieh, "Adaptive system-level fault diagnosis of bijective connection networks," *IEEE Trans. Rel.*, vol. 74, no. 2, pp. 2916–2926, Jun. 2025, doi: 10.1109/TR.2024.3425759.
[23] L. Lin, S. Zhou, and S.-Y. Hsieh, "Neural network enabled intermittent fault diagnosis under comparison model," *IEEE Trans. Rel.*, vol. 72, no. 3, pp. 1206–1219, Sep. 2023, doi: 10.1109/TR.2022.3199504.
[24] J. Song, L. Lin, Y. Huang, and S.-Y. Hsieh, "Intermittent fault diagnosis of split-star networks and its applications," *IEEE Trans. Parallel Distrib. Syst.*, vol. 34, no. 4, pp. 1253–1264, Apr. 2023, doi: 10.1109/TPDS.2023.3242089.
[25] M. Lv, X. Liu, H. Dong, and W. Fan, "Reliability analysis of complete cubic networks based on extra conditional fault," *J. Supercomput.*, vol. 80, pp. 21952–21974, Jun. 2024, doi: 10.1007/s11227-024-06272-w.
[26] L. Yang, S. Zhou, and E. Cheng, "The (t,k)-diagnosability of cayley graph generated by 2-tree," *J. Parallel Distrib. Comput.*, vol. 200, 2025, Art. no. 105068, doi: 10.1016/j.jpdc.2025.105068.
[27] E. Cheng, M. Lipman, and L. Lipták, "Strong structural properties of unidirectional star graphs," *Discrete Appl. Math.*, vol. 156, no. 15, pp. 2939–2949, Aug. 2008, doi: 10.1016/j.dam.2007.12.005.
[28] B. Li, J. Lan, W. Ning, Y. Tian, X. Zhang, and Q. Zhu, "h-extra r-component connectivity of interconnection networks with application to hypercubes," *Theor. Computer Sci.*, vol. 895, pp. 68–74, Dec. 2021, doi: 10.1016/j.tcs.2021.09.030.
[29] W. Liu, J. Liu, J.-M. Chang, J. Wu, and Q. Wang, "A novel fault-tolerant technique for star graph-based interconnection networks," *J. Supercomput.*, vol. 81, 2025, Art. no. 820, doi: 10.1007/s11227-025-07272-0.
[30] R. P. Ziwich and E. P. Duarte, "A nearly optimal comparison-based diagnosis algorithm for systems of arbitrary topology," *IEEE Trans. Parallel Distrib. Syst.*, vol. 27, no. 11, pp. 3131–3143, Nov. 2016, doi: 10.1109/TPDS.2016.2524004.
[31] C.-K. Lin, T.-L. Kung, and J. J. Tan, "An algorithmic approach to conditional-fault local diagnosis of regular multiprocessor interconnected systems under the PMC model," *IEEE Trans. Comput.*, vol. 62, no. 3, pp. 439–451, Mar. 2013, doi: 10.1109/TC.2011.249.
[32] T.-L. Ye and S.-Y. Hsieh, "A scalable comparison-based diagnosis algorithm for hypercube-like networks," *IEEE Trans. Rel.*, vol. 62, no. 4, pp. 789–799, Dec. 2013, doi: 10.1109/tr.2013.2284743.
[33] S. Zhou, L. Lin, L. Xu, and D. Wang, "The t/k-diagnosability of star graph networks," *IEEE Trans. Comput.*, vol. 64, no. 2, pp. 547–555, Feb. 2015, doi: 10.1109/tc.2013.228.
[34] M. Lv, S. Zhou, G. Chen, L. Chen, J. Liu, and C.-C. Chang, "On reliability of multiprocessor system based on star graph," *IEEE Trans. Rel.*, vol. 69, no. 2, pp. 715–724, Jun. 2020, doi: 10.1109/TR.2019.2919282.
[35] Z. Wan, L. Lin, Y. Huang, and S.-Y. Hsieh, "Component diagnosis strategy of star graphs interconnection networks," *IEEE Trans. Rel.*, vol. 73, no. 4, pp. 1907–1917, Dec. 2024, doi: 10.1109/TR.2024.3357700.

Wenfei Liu received the B.Eng. degree from Zhangjiakou University, Zhangjiakou, China, in 2023. He is currently working the master's degree in software engineering with Guangxi Normal University, Guilin, China. His research interests include network and information security, fault diagnosis, and graph theory algorithms.

Jiafei Liu received the B.S. degree from Zhoukou Normal University, Zhoukou, P.R. China, in 2017, and the Ph.D. degree from Fujian Normal University, Fuzhou, P.R. China, in 2022. He is currently working with the School of Computer Science and Engineering, Guangxi Normal University. He was awarded for the Guangxi Qingmiao Talent Program in 2024 and the Guangxi Young Elite Scientists Sponsorship Program in 2025. His research interests include network reliability, fault-tolerant computing, algorithms, and interconnection networks. He has published more than 30 papers, and has served as a Reviewer including IEEE TRANSACTIONS ON COMPUTERS, IEEE TRANSACTIONS ON RELIABILITY, THEORETICAL COMPUTER SCIENCE, *Discrete Applied Mathematics*, and other publications.

Eddie Cheng received the Ph.D. degree from the University of Waterloo, Canada, in 1995. After spending two years at Rice University, he joined Oakland University where he is currently a Distinguished Professor of Mathematics. He served as the Chair of the Department of Mathematics and Statistics from 2010 to 2013. He has won a number of awards including the 2009 Presidents Council State Universities of Michigan Distinguished Professor of the Year Award and the 2018 University of Waterloo Faculty of Mathematics Alumni Achievement Medal. He is the Co-Editor-in-Chief of *International Journal of Computer Mathematics: Computer Systems Theory* (Taylor & Francis) and the Editor-in-Chief of *Journal of Interconnection Networks* (World Scientific), as well as an Editorial Board Member of many other journals.

Sun-Yuan Hsieh (Fellow, IEEE) received the Ph.D. degree in computer science from the National Taiwan University, Taipei, Taiwan, in 1998. He is currently a Chair Professor with the National Cheng Kung University, Tainan, Taiwan. His research interests include fault-tolerant computing, bioinformatics, parallel and distributed computing, and algorithmic graph theory. He is currently an experienced Editor with editorial services to a number of journals, including serving as an Associate Editor for IEEE TRANSACTIONS ON COMPUTERS, IEEE TRANSACTIONS ON RELIABILITY, *Journal of Computer and System Science*, *Theoretical Computer Science*, *Discrete Applied Mathematics*, *Journal of Supercomputing,* an Editor-in-Chiefs of the *International Journal of Computer Mathematics, Discrete Mathematics, Algorithms and Applications*, and a Managing Editor for the *Journal of Interconnection Networks*.

Jingli Wu received the B.S. degree in computer software and the M.S. degree in control theory and control engineering from Guangxi University, and the Ph.D. degree in computer application from the Central South University. He she a Professor with the College of Computer Science and Information Engineering, Guangxi Normal University. Her research interests include bioinformatics and intelligent optimization algorithm.

Gaoshi Li received the Ph.D. degree in computer science and technology from the Central South University, Changsha, China, in 2019. He is currently an Associate Professor with the Key Lab of Education Blockchain and Intelligent Technology, Ministry of Education & Guangxi Key Lab of Multisource Information Mining & Security and College of Computer Science and Engineering, Guangxi Normal University. His research interests include bioinformatics, computational biology, and machine learning.